Eur. Phys. J. D **25**, 113–121 (2003)
DOI: 10.1140/epjd/e2003-00096-6

THE EUROPEAN PHYSICAL JOURNAL D

The g_J-factor in the ground state of Ca^+

G. Tommaseo[1], T. Pfeil[1], G. Revalde[2], G. Werth[1,a], P. Indelicato[3,b], and J.P. Desclaux[4]

[1] Johannes Gutenberg Universität, Institut für Physik, 55099 Mainz, Germany
[2] Institute of Atomic Physics and Spectroscopy, University of Latvia, Raina Blvd. 19, Riga, Latvia
[3] Laboratoire Kastler Brossel, École Normal Supérieure et Université Pierre et Marie Curie, Case 74, 4 place Jussieu, 75005 Paris, France
[4] 15 chemin du Billery, 38360 Sassenage, France

Received 9 December 2002 / Received in final form 24 February 2003
Published online 29 April 2003 –

Abstract. We have determined the g_J-factor of the Ca^+ ion in the electronic $4S_{1/2}$ ground state on a cloud of ions confined in a Penning trap with a superimposed magnetic field of 1.43 T. We use a c.w. laser to prepare a Zeeman substate by optical pumping and induce $\Delta m_J = 1$ transitions by a resonant microwave field at 40 GHz. Resonance is detected by a change in the fluorescence intensity originating from the ion cloud. We obtain a full width in the resonance of a few kHz and the fractional uncertainty of the line center, taking the average of several measurements, was 4×10^{-8}. After calibrating the magnetic field by the cyclotron frequency of electrons stored in the same trap we obtain as result $g_J = 2.002\,256\,64(9)$. The result is supported by a relativistic Multi-Configurational Dirac-Fock calculation.

PACS. 32.60.+i Zeeman and Stark effects – 32.10.Dk Electric and magnetic moments, polarizability

1 Introduction

The g-factor relates the magnetic moment μ of a system to its angular momentum J by the relation

$$\mu = g\frac{e\hbar}{2m}J \tag{1}$$

where e and m are the charge and the mass of the system, respectively. Measurements of g in atomic systems have provided a means of checking theoretical predictions of relativistic quantum mechanics. The g-factor deviates for bound systems from the value of the free electron by a number of contributions. For light atoms the main contribution is the relativistic kinetic correction $\delta g_{\rm rel}$, first introduced by Breit [1]. In heavy atoms the core-valence correlation correction $\delta g_{\rm corr}$ dominates [2]. The Breit interaction $\delta g_{\rm Br}$ between the valence and core electrons also gives a significant contribution [3]. Bound-state quantum electrodynamic corrections are generally considered as small except for hydrogen like systems [4]. g_J-factors of neutral atoms have been measured with great precision particularly for the alkali atoms. Here the comparison between theory and experiment can be made on the 10^{-6} level of accuracy since the single valence electron of these systems allows to obtain accurate wavefunctions using MCDF-Method (Multiconfiguration Dirac-Fock) and RMBPT (Relativistic Many Body Perturbation Theory).

Alkali like atomic ions are equally well suited to test the corresponding atomic physics calculations. Precise values of g_J-factors for some ions have been obtained in recent years using microwave-optical double resonance method, combined with the ion storage technique [5]. The ions are confined in Penning traps with a superimposed strong magnetic field. The storage of small ion clouds for virtually unlimited time under high vacuum conditions has a number of advantages: the precision of induced transitions between long lived ionic energy levels is not limited by the finite observation time. The small trapping volume of at most a few mm^3 makes it comparatively easy to obtain high spatial homogeneity of the magnetic field over the region of interest. The use of superconducting magnets assures at the same time high temporal stability. In case of microwave transitions, the first order Doppler effect does not broaden the spectral line in spite of the fact that the average kinetic energy of trapped ions is typically of the order of a few eV when no cooling methods are applied and thus much higher than in experiments on neutral atoms. The ion motion in traps leads to an unshifted and unbroadened central line and to sidebands at the ion oscillation frequencies. This is due to the fact that the amplitude of the ion oscillation in the trap is in general smaller than the wavelength of the inducing radiation (Dicke effect) [6]. Finally collisions with neutral background atoms which may shift the resonance frequencies play a negligible role at pressures below 10^{-5} mbar.

The determination of ionic g_J-factors in Penning traps has been restricted so far to alkali-like systems because

[a] e-mail: werth@mail.uni-mainz.de
[b] e-mail: paul.indelicato@spectro.jussieu.fr

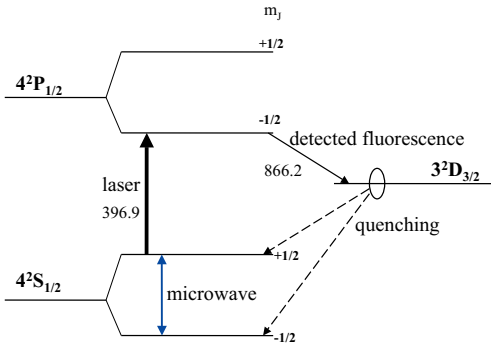

Fig. 1. Partial level scheme of Ca^+ showing the Zeeman splitting of the ground level and the radiation fields for the double resonance experiment. The transition wavelengths are given in nm.

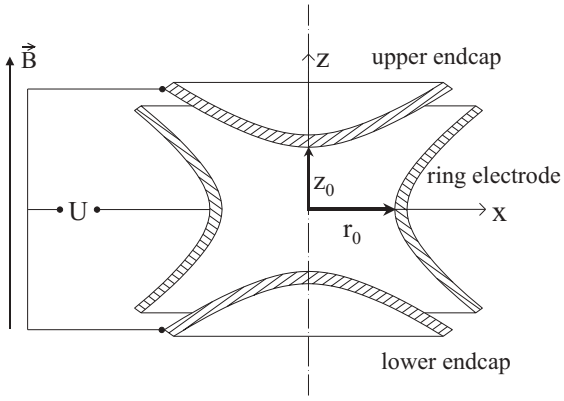

Fig. 2. Electrode configuration of the hyperbolic Penning trap.

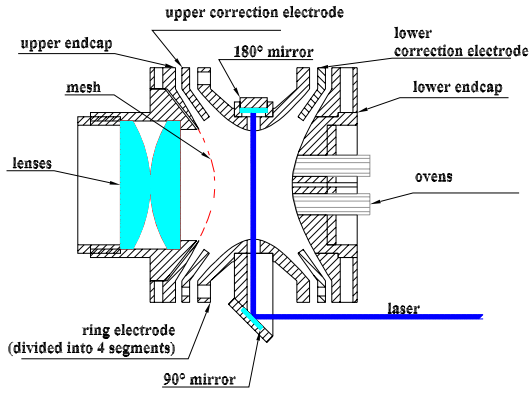

Fig. 3. Technical sketch of the Penning trap as used in our experiment.

of their simple level structure and their strong resonance lines for laser excitation: Be^+ [7], Mg^+ [8], Ba^+ [9] and Hg^+ [10]. In all cases the relative uncertainty in g_J was below 10^{-7}.

Here we report about an experiment to determine the g_J-factor of Ca^+ in the electronic $4S_{1/2}$ ground level. The positive Ca ion represents an ideal object for spectroscopic measurements. The lowest energy level accessible by electric dipole transitions are the $4P_{1/2}$ and $4P_{3/2}$ levels at 397 nm and 393 nm, respectively, above the $4S_{1/2}$ ground state. In between there are two low lying states, $3D_{3/2}$ and $3D_{5/2}$, at 729 nm and 731 nm distance from the ground level. They decay by electric quadrupole radiation and their lifetime has been measured to about 1 s [11,12]. In our experiment the $4S_{1/2}$, $4P_{1/2}$ and $3D_{3/2}$ levels are involved which form a Λ-type level scheme (Fig. 1). All wavelength necessary to access the excited states can be produced by commercially available c.w. lasers. With lasers having a small spectral band width it is possible to deplete single Zeeman sublevels by optical pumping and to perform double and triple resonance experiments.

From the theoretical point of view, this light alkali-system represents a challenge to calculations. Since Ca^+ can be regarded as a nearly neutral system correlation effects can be large. This is due to the fact that the electronic contributions scale as $1/Z_{\rm eff}$ compared to the leading term which scales as $Z_{\rm eff}^2$ [13]. The important effect of the 19 electrons is in this context to reduce $Z_{\rm eff}$ to something much smaller than $Z = 20$.

2 Experiment

The experimental set-up consists mainly of an ultrahigh vacuum apparatus made of stainless steel. An ion getter pump maintains after bake-out a base pressure below 10^{-9} mbar. The heart of the apparatus — the ion trap — is placed inside a glass tube of 90 mm diameter. This tube is located in the horizontal room temperature bore of a superconducting magnet and the trap is placed at the position of maximal field strength and lowest inhomogeneity.

The ion trap is made of oxygen free high vacuum suitable copper and has hyperbolic shaped electrodes of characteristic dimension $d_0 = \sqrt{r_0^2 + 2z_0^2} = 1.5$ cm, r_0 being the radius of the ring electrode and $2z_0$ the distance between the two endcap electrodes (see Fig. 2). The trap has been provided with correction electrodes in order to minimize electrical higher order perturbation terms which can cause a distortion of the ideal quadrupole potential. These perturbations are mainly due to the fact that the surfaces of the trap electrodes haven't got a perfect hyperbolic shape. Additionally the quadrupolar trapping field is distorted by the holes in the electrodes which are necessary to perform laser spectroscopic measurements with the stored ions. The ring electrode is divided into four quadrants, between which an additional r.f. field can be applied, needed to center the ions as described below. The upper endcap is made of a mesh which allows to detect the fluorescence photons of the laser excited ions and has a transmission coefficient of about 72%. The lower endcap contains two cylindrical ceramic tubes with holes where we put a small macroscopic quantity of a metallic calcium probe. A sketch of our trap is shown in Figure 3. Ions are created by ionization of neutral Ca atoms inside the trap caused by electrons coming from a rhenium filament which goes through the holes of the ceramic tubes of the oven. This filament is also used to evaporate the atoms from

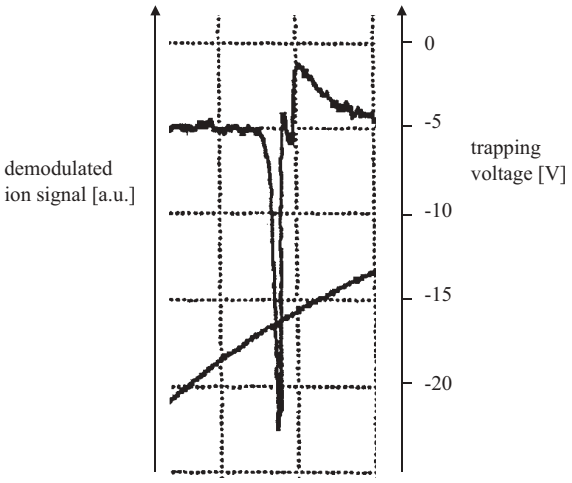

Fig. 4. Electronic detection signal of stored ions. The voltage drop across a tank circuit is plotted *vs.* the ramped trapping voltage (lower trace), showing damping signals from stored ions. The large (negative) peak is due to ions of mass 41. Ca^+ ions of mass 40 appear as a small signal on the right side of mass 41.

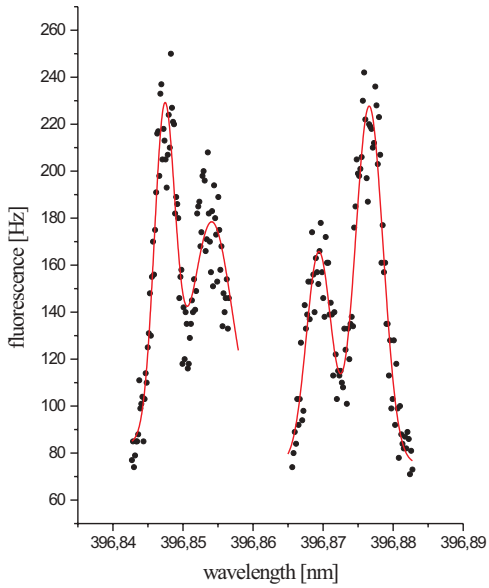

Fig. 5. Laser scan across the $4S_{1/2}-4P_{1/2}$ resonance transition of Ca^+ in a magnetic field of 1.43 T. The splitting of the two left and two right maxima of the observed fluorescence photon number corresponds to the Zeeman separation of the excited $4P_{1/2}$ state. Taking the notation of Figure 1 the outer peaks are the $\sigma^{\pm}$-transitions and correspond to $4^2S_{1/2}, m_J = \pm 1/2 \longrightarrow 4^2P_{1/2}, m_J = \mp 1/2$, whereas the inner peaks are the π-transitions corresponding to $4^2S_{1/2}, m_J = \pm 1/2 \longrightarrow 4^2P_{1/2}, m_J = \pm 1/2$. The difference between the first and third and also between the second and fourth maximum (from left) is therefore the Zeeman separation of the $4S_{1/2}$ ground state.

the metallic probe. Heating the oven for a few seconds was sufficient to fill the trap with ions to the space charge limit which was estimated to occur at about 10^6 ions. The ions were detected in two different ways: (a) observation of fluorescence photons from the decay of the laser excited $P_{1/2}$ level into the $D_{3/2}$ state at 866 nm. Although the branching ratio of this decay compared to the decay back to the ground state is only 1:16 [14,15] it has the advantage that it is free of laser stray light background which is blocked by an interference filter. (b) Observation of the induced voltage in the endcap electrodes from the axial ion oscillation. This voltage can be detected as damping of a narrow band amplifier tuned to the ions axial oscillation frequency and connected across the endcaps. It gives a signal proportional to the stored ion number as shown in Figure 4.

The laser beam, produced by a frequency doubled Ti:Sa laser, was guided into the apparatus parallel to the magnetic field lines of the solenoid, however off axis. It was deflected into the trap by 90° with a mirror (see Fig. 3). After passing through the trap it was reflected back into itself by a second mirror and left the apparatus.

A lens system situated in the upper endcap of the trap provides the collection of the fluorescence photons. These are then focused into a light pipe and guided to a GaAs photomultiplier placed at about 1 m from the magnet. A single-photon counting system connected to a personal computer takes up the fluorescence rate. The overall detection efficiency including solid angle, transmission losses and finite photomultiplier efficiency was about 10^{-5}.

If the ions are excited at saturation rate, which occurs at a laser power density of a few mW/cm^2, one would expect a fluorescence photon number in the order of 10^6 photons per second from a single ion, resulting from the radiative lifetime of the $4P_{1/2}$ of 7 ns [16] and the branching rate of the $4S_{1/2} - 3D_{3/2}$ transition. Then however, population trapping would occur in the long lived $3D_{3/2}$ state. We reduced the effective lifetime of this state by operating the trap at background pressures of typically 10^{-3} mbar, using He as buffer gas. Quenching collisions reduce the $3D_{3/2}$-lifetime to the ms range level [17,18]. The expected photon number then is of the order of 10^3 s^{-1} from a single ion. This number is reduced by an order of magnitude since the ion cloud diameter is about 4 mm, whereas the laser beam diameter was only 1 mm. Considering the overall detection efficiency of 10^{-5} one would the expect a recorded photon count rate of about 10^3 s^{-1} from 10^6 ions. The observed photon number, however, was by about one order of magnitude below the expectations as seen from Figure 5. The electronic detection signal revealed that only a small fraction of the trapped ions had the mass 40 as expected for Ca^+. The mass can be determined by a measurement of the mass dependent axial oscillation frequency

$$\omega_z = \sqrt{\frac{4eV}{m\,{d_0}^2}}. \qquad (2)$$

When we sweep the trapping voltage different mass ions are brought into resonance with the tuned detection circuit and give rise to damping signals at different voltages. As seen from Figure 4 we found that a strong signal appeared at mass 41 and the mass 40 signal was only of

marginal size, typically of a few % of the strong 41-mass signal. We observed that along with the heating of the oven the partial pressure of hydrogen in the vacuum system rose substantially and we concluded that a chemical reaction took place which eliminated most of the Ca^+ ions by formation of CaH^+. Attempts to locate and remove the source of hydrogen from the system were unsuccessful. We compensated for the substantial loss in count rate by longer averaging times.

When we sweep the laser frequency across the $4S_{1/2}-4P_{1/2}$ transition we record spectra as shown in Figure 5. The averaging time for such a spectrum was 20 min. It shows the Zeeman splitting of the $4S_{1/2}$- and $4P_{1/2}$-states of 40 GHz and 13 GHz, respectively, in our B-field of 1.43 T. The linewidth of about 7 GHz is caused by first order Doppler broadening from the ion motion in the trap which corresponds to a temperature of 6350 K.

The storage time of ions in a Penning trap is limited by collisions with background gas molecules since one of the ion oscillations, the magnetron motion at frequency

$$\omega_m = \frac{\omega_c}{2} - \sqrt{\frac{{\omega_c}^2}{4} - \frac{{\omega_z}^2}{2}} \qquad (3)$$

increases its radius under the influence of collisions and the ions get lost from the trap. $\omega_c = eB/m$ is the free ions cyclotron frequency. At a base pressure of 10^{-9} mbar in our apparatus we achieved typical storage times of the order of 20 min. Adding background gases at higher pressures as required for collisional quenching of the metastable D-level would reduce the storage time to a level which would not allow significant averaging of the optical signal. The storage time, however could be substantially increased by applying a technique which drives the ions into center of the trap [19,20]. An additional radio-frequency field at the sum of ω_m and of the reduced cyclotron motion frequency

$$\omega_c' = \frac{\omega_c}{2} + \sqrt{\frac{{\omega_c}^2}{4} - \frac{{\omega_z}^2}{2}} \qquad (4)$$

is applied to adjacent segments of the ring electrode. The effect of this field is to couple the magnetron motion to the reduced cyclotron motion. The reduced cyclotron motion is damped by collisions with neutral molecules and its amplitude is decreased. The coupling to the magnetron motions provides that the damping overcompensates the increase of the magnetron orbit. As a result the ions spiral towards the trap center and aggregate there. The storage time is then extended and in our experiment we obtain typically 24 h. An additional benefit of the collisions is that the ions temperature is somewhat reduced by interaction with the neutral atoms at room temperature.

3 Measurements

We determined the ground state g_J-factor of Ca^+ by the method of microwave optical double resonance: one of the Zeeman ground levels was selectively depleted by laser excitation and repopulated by induced transitions from the adjacent Zeeman state (Fig. 1). The Zeeman splitting in the $4S_{1/2}-4P_{1/2}$ optical transition was easily resolved as seen from Figure 5. The magnetic field of 1.43 T was chosen because a low noise klystron for the ground state separation of 40 GHz was available in our lab. The klystron frequency was phase locked to a quartz oscillator whose time base was provided by a Rb atomic frequency standard. The microwaves were guided into the apparatus using a waveguide and a semiflexible cable which was connected to the filament of one of the ovens, serving as antenna. Induced resonance transitions between the two Zeeman states $m_J = +1/2$ and $m_J = -1/2$ of the ground state were detected by an increase of the fluorescence intensity. Typical count rates at resonant excitation depend on the microwave amplitude. At high amplitudes they were of the order of 10 s^{-1} compared to the photomultiplier dark counts of 2 s^{-1}. Laser stray light was completely negligible. To reduce statistical scatter of the data we added the counts of a few hundred sweeps of the microwave field across the resonance. The total time to record one spectral line was of the order of 1 h. We recorded spectra at different power levels of the microwave field to account for possible power broadening. The final line width would be given by the inhomogeneity of the magnetic field over the volume of the ion cloud. According to the specifications of our magnet, one might expect a relative line width of the order of 10^{-8}. The narrowest line width which we actually observed in our experiment was 3 kHz (Fig. 6) corresponding for a fractional width of 8×10^{-8}. Further reduction of the microwave power made the signal too small to distinguish it from the background in a reasonable time.

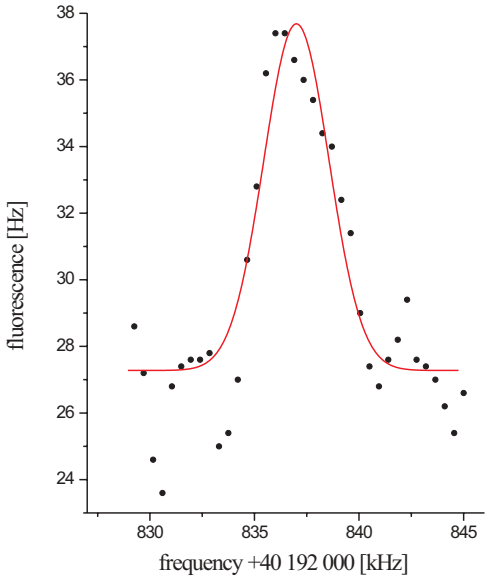

Fig. 6. Narrowest observed induced Zeeman transition in the ground state at 40 GHz. The full line width is 3 kHz. A Lorentzian line shape is fitted to the experimental data.

We found it very difficult to reproduce line of a few kHz width with signal strength just above the noise level, which was due to fluctuations in the microwave power

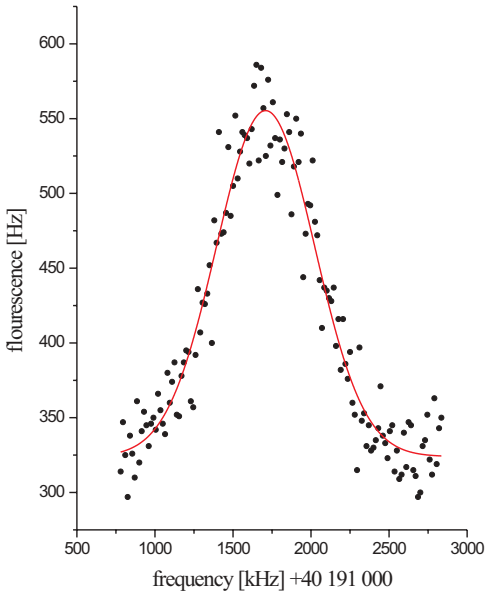

Fig. 7. Typical resonance line for induced ground state Zeeman transitions as used for the evaluation of the g_J-factor. The center line can be determined to 9 kHz corresponding to a fractional uncertainty of 2.2×10^{-7}. A Lorentzian line shape is fitted to the experimental data.

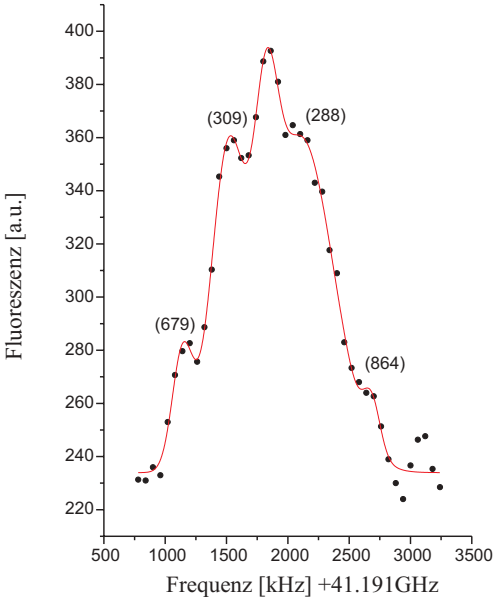

Fig. 8. Sideband structure in the Zeeman spectrum of Ca^+ measured at a magnetic field of 1.43 T. The numbers in round brackets give the distance from the central line in kHz.

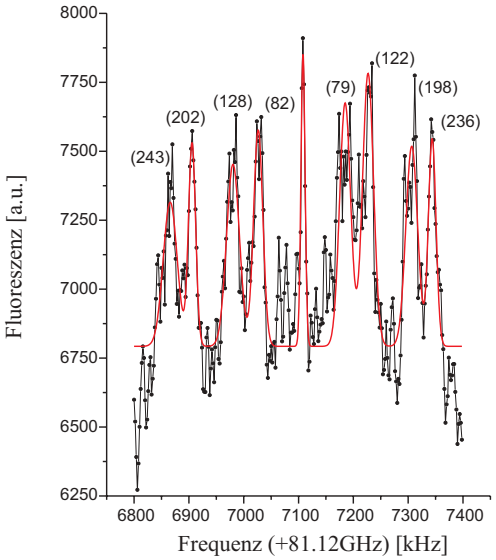

Fig. 9. Sideband structure in the Zeeman spectrum of Ba^+ measured at a magnetic field of 2.87 T. The numbers in round brackets give the distance from the central line in kHz.

while scanning the microwave field across the Zeeman resonance. We decided therefore to increase the power to an amount where the signal was relatively strong and the statistical scatter allowed easy fitting of theoretical lineshapes to the data. A typical linewidth was a few hundred kHz. An example is shown in Figure 7. The least square fitting procedure to a Lorentzian line shape gave statistical uncertainties of the order of 9 kHz. Taking the weighted mean value of the center frequency of 24 single measurements the relative uncertainty could be reduced to 2 kHz. This corresponds to a fractional uncertainty in the determination of the Zeeman splitting of about 5×10^{-8}.

3.1 Line shape of the Zeeman resonance

We have observed a substructure in the Zeeman spectrum of our optical-microwave double resonance experiment showing sidebands symmetrically arranged around the central peak of the Zeeman transition (Fig. 8). Because of the poor signal-to-noise ratio in our Ca^+ experiment the sideband structure is not well resolved. Therefore we used in addition previous similar measurements on Ba^+ ions [9] for line shape analysis (Fig. 9). The central line is in first order not Doppler broadened because of the Dicke criterion, *i.e.* the wavelength of the microwave field is much larger than the amplitude of the ion motions. Similar sideband structures were observed by Schuessler [21] and Enders [22] in a Paul trap.

The sideband structure has its origin in the irradiated microwaves which form a standing electromagnetic field inside the Penning trap. The trap acts therefore as a microwave cavity and the ions see at different times a frequency and amplitude modulated field. The interaction between the ion motion and the standing microwave field can be described by introducing an formalism based on correlation functions [23,24].

The starting point of the calculation is the Wiener-Khintchine theorem [25,26] which gives a relationship between the spectral power density of the Zeeman transition and the correlation function describing the standing microwave field. The spectral power density results from

a Fourier transformation of the correlation function:

$$P(\omega,\omega_0)=\frac{1}{\pi}\int_{-\infty}^{\infty}G_{pq}(\tau)\mathrm{e}^{\mathrm{i}\omega_0\tau}\mathrm{d}\tau \tag{5}$$

with

$$\omega_0=\frac{E_q-E_p}{\hbar}$$

being the microwave resonance frequency between two Zeeman sublevels $|p\rangle$ and $|q\rangle$. In our case is

$$|p\rangle\equiv|4^2\mathrm{S}_{1/2},m_J=-\frac{1}{2}\rangle \quad \text{and}$$
$$|q\rangle\equiv|4^2\mathrm{S}_{1/2},m_J=+\frac{1}{2}\rangle.$$

The correlation function G_{pq} is given by:

$$G_{qp}(\tau)\equiv A_{qp}\langle\mathcal{H}(t+\tau)\mathcal{H}(t)\rangle \tag{6}$$

A_{pq} is a constant describing the matrix elements of the magnetic dipole moments of the stored ions. $\mathcal{H}(t)$ represents the microwave field which can be expressed with the help of Bessel functions

$$J_n(x)=\sum_{l=0}^{\infty}\frac{(-1)^l}{l!(n+l)!}\left(\frac{x}{2}\right)^{n+2l} \tag{7}$$

considering that the standing electromagnetic field inside the trap develops mainly in the cylindrical TE_{013} mode [27]. The axial and the radial components of the microwave field are respectively given by:

$$H_z=H_1J_0(k_1r)\cos(k_3z)\cos\omega t \tag{8}$$
$$H_r=\tilde{H}_1J_1(k_1r)\sin(k_3z)\cos\omega t. \tag{9}$$

The microwave field $\mathcal{H}(t)$ is then the superposition of the axial and the radial component. r and z represent the known solution of the ion trajectories in the Penning trap

$$z=|A_z|\{\cos(\omega_z t)+\sin(\omega_z t)\} \tag{10}$$
$$r=\sqrt{|A_+|^2+|A_-|^2+2|A_+||A_-|\cos(\omega_c'-\omega_m)t} \tag{11}$$

$|A_z|$, $|A_+|$ and $|A_-|$ being the amplitude of the axial, the reduced cyclotron and the magnetron motion, respectively. The correlation function finally results in

$$G_{qp}=A_{qp}\int_0^{|A_+|}\mathrm{d}|A_+|\int_0^{|A_-|}\mathrm{d}|A_-|\int_{-|A_z|}^{|A_z|}\times\mathrm{d}|A_z|\;\mathcal{H}(t)\mathcal{H}(t+\tau)\eta \tag{12}$$

η stands for the velocity distribution of the ion cloud. This function must be chosen appropriately. The expression in equation (12) can be analytically solved by assuming for η a Maxwell-Boltzmann distribution. By inserting this result in equation (5) we get a nonvanishing solution when the following conditions for the frequency ω are fullfilled:

$$\begin{aligned}
&\{1\}\quad \omega=\omega_0\pm 2n\omega_z\\
&\{2\}\quad \omega=\omega_0\pm(2n-1)\omega_z\\
&\{3\}\quad \omega=\omega_0\pm n(\omega_+-\omega_-)\\
&\{4\}\quad \omega=\omega_0\pm n(\omega_+-\omega_-)\pm 2m\omega_z\\
&\{5\}\quad \omega=\omega_0\mp n(\omega_+-\omega_-)\pm 2m\omega_z\\
&\{6\}\quad \omega=\omega_0\pm n(\omega_+-\omega_-)\pm(2m-1)\omega_z\\
&\{7\}\quad \omega=\omega_0\mp n(\omega_+-\omega_-)\pm(2m-1)\omega_z\\
&\qquad \text{with}\quad n,m\in\mathbb{N}\diagdown\{0\}.
\end{aligned} \tag{13}$$

Table 1. Frequency position of the sidebands in the Ca^+ Zeeman spectrum. For the experimental values the average of left and right sidebands are taken.

	Position from central peak [kHz]		
# in Eqs. (13)	Experiment	Theory	Combination
{5}	298(25)	289	$(\nu_+-\nu_-)-2\nu_z$
{4}	771(19)	753	$(\nu_+-\nu_-)+2\nu_z$

Table 2. Frequency position of the sidebands in the Ba^+ Zeeman spectrum. For the experimental values the average of left and right sidebands are taken.

	Position from central peak [kHz]		
# in Eqs. (13)	Experiment	Theory	Combination
{5}	80(1)	82	$5(\nu_+-\nu_-)-6\nu_z$
{7}	125(2)	132	$6(\nu_+-\nu_-)-7\nu_z$
{5}	201(1)	200	$4(\nu_+-\nu_-)-4\nu_z$
{7}	240(2)	232	$8(\nu_+-\nu_-)-9\nu_z$

Tables 1 and 2 give a comparison between the theoretically determined and the measured positions of the sidebands showing a good agreement for Ca^+ and Ba^+, respectively. The obvious asymmetry of the line in Figure 8 arises from incomplete optical pumping during the scan of the microwaves and vanishes when scans with different sweep directions are added. A detailed theoretical treatment of the phenomena is described in [28]. A fit of our data with a line shape formula containing sidebands does, however, not improve the accuracy of the center frequency. We use therefore the simple Lorentzian line shape for evaluation of our data.

3.2 Magnetic field calibration

The Zeeman splitting $\Delta E_{\mathrm{Zeeman}}$ is related to the g_J-factor by

$$h\nu_{\mathrm{Zeeman}}\equiv\Delta E_{\mathrm{Zeeman}}(4^2\mathrm{S}_{1/2},\Delta m_J=1)=g_J\mu_B B \tag{14}$$

$\mu_B=e\hbar/2mc$ is the Bohr magneton. In order to obtain g_J we need to know the magnetic field B at the ions' position. A calibration of the field is performed by measuring the cyclotron frequency of electrons stored in the same trap after reversing the sign of the trapping voltage. The electrons are electronically detected in a similar manner

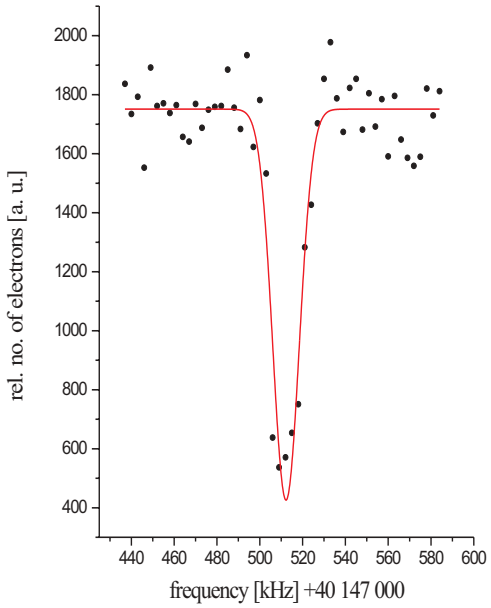

Fig. 10. Cyclotron resonance of stored electrons for calibration of the magnetic field.

as the ions by their induced voltage in the endcap electrodes of the trap. The axial oscillation frequency of the electrons was in our experiment at 12 MHz. Excitation of the cyclotron motion and transfer of the increased electron energy to other modes of oscillation lead to a loss of electrons from the trap which serves to monitor resonant excitation of the cyclotron frequency. For a magnetic field of 1.43 T this frequency is 40 GHz, very close to the Zeeman transition frequency. Therefore we were able to use the same microwave source for excitation. When we plot the electron signal height *vs.* microwave frequency we observe a minimum in the detection signal whose width is of the order of 10 kHz (Fig. 10). The center frequency can be determined to about 10% of the width. After averaging over 20 measurements taken before and after the Zeeman resonance measurements, the uncertainty of the mean value was of the order of 200 Hz, corresponding to relative uncertainty in the determination of the center frequency of 5×10^{-9}.

4 Results and discussion

The ratio of the Zeeman resonance frequency ν_{Zeeman} to the cyclotron frequency of the electrons $\nu_c = eB/2\pi\, m$ scaled with a factor of 2 gives directly the g_J-factor. The number which we obtain from the measurements may be affected by systematic shifts. The main reason for such a shift could be a temporal drift of the magnetic field. This drift has been measured for our magnet and the amounts to $\delta B/B = 1 \times 10^{-9}$/h. We have measured the electrons cyclotron frequency before and after the Zeeman measurements. The statistical scatter of 20 single measurements showed Gaussian distributions whose mean values differed by less than 4×10^{-9}. This is much less than the statistical uncertainty of the Zeeman resonances and therefore any shifts resulting from a magnetic field shift can be neglected.

The cyclotron resonance of the electrons is not an eigenfrequency of the motion but appears as a sideband to the perturbed cyclotron frequency ω_c'. The difference between the two frequencies is the magnetron frequency ω_m which amounts for our conditions to 685 Hz for a trapping voltage of 1 V. This difference can not be resolved in our measurements of the cyclotron frequency. If we reasonably assume that the measured frequency occurs at the average of ω_c' and ω_c we have to correct the cyclotron frequency by 8×10^{-9} which is negligible compared to the statistical uncertainty of the Zeeman transition frequency. Finally a possible shift of the electrons' cyclotron frequency can appear from relativistic shifts. The initial electron temperature after the loading of the trap is approximately 1/10 of the total potential depth of the trap. It is 1.25 eV, when we apply 25 V at the ring electrode and keep the endcaps at ground potential. The electrons lose energy by synchrotron radiation. The time constant for exponential energy loss at our field of 1.43 T is 1250 ms. In order to reduce the relativistic shift we waited several seconds after loading before we irradiated the electrons with the microwave field. Moreover the trap potential was reduced from initially 25 V to 1 V before irradiation in order to remove hot electrons from the trap. We can reasonably assume that the remaining electron cloud is in thermal equilibrium with the environment at room temperature. This assumption is based on three considerations: first of all synchrotron radiation, as reported in the "geonium paper" [29], is the dominant mechanism of energy loss of the electrons. Kienow *et al.* [30] report a narrowing of the energy distribution due to synchrotron radiation cooling for longer storage times of the electrons. So by taking a waiting time of $4s$ which is much longer then the time constant for exponential energy loss we can be sure that the electrons are in thermal equilibrium with the environment. Because the Penning trap uses only static electric and magnetic fields we do not expect any heating mechanism for the electrons. Finally the presence of background gas in the apparatus contributes to the thermalization of the electrons as well. The relativistic shift amounts then to 5×10^{-8} which we apply to our data.

No correction is applied to the Zeeman resonances. Taking the measured values for ν_c and ν_{Zeeman}, applying the above mentioned corrections to ν_c and adding the uncertainties in quadrature we obtain as final result for the g_J value:

$$g_J(4^2\mathrm{S}_{1/2}, \mathrm{Ca}^+) = 2\,002\,256\,64(9).$$

The experimental fractional uncertainty of 4.5×10^{-8} is of the same order as in previous cases of measurements on alkali-like ions using ion traps.

5 Theoretical considerations

The theoretical evaluation of the g-factor of the Ca^+ ion is a difficult task that requires the use of fully relativistic

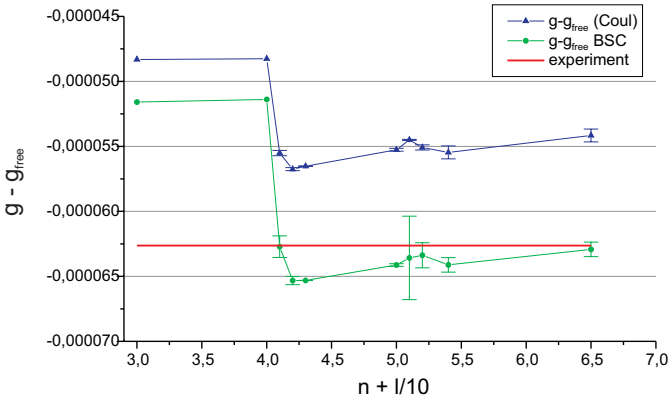

Fig. 11. Convergence of MCDF calculation of the bound contribution to the Ca^+ g-factor as a function of $n + \ell/10$. The width of the horizontal line for the experimental value corresponds to the experimental uncertainty.

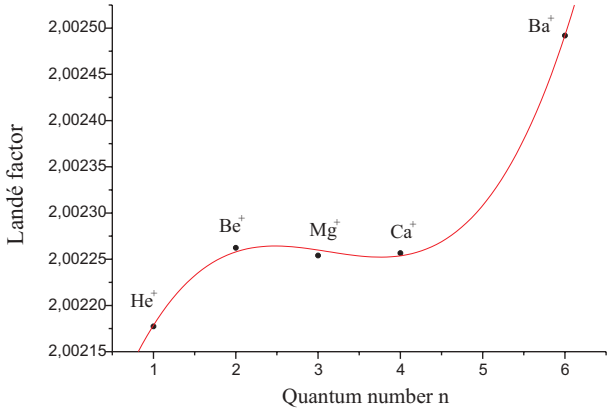

Fig. 12. Evolution of the Landé-factor alkali-like ions *vs.* the quantum number n. It demonstrates the importance of correlation effects in these systems. The g-factor for the elements Sr^+ ($n = 5$) and Ra^+ ($n = 7$) would complete the series.

techniques. Relativistic Many-Body Perturbation Theory calculations of Ba^+ have been performed some years ago [3] providing a good agreement with experiment. This calculation involved single and double excitations. The calculations showed the importance of proper account of the Breit term in the electron-electron interaction. In this subsection, we report a Multiconfiguration Dirac-Fock calculation (MCDF) of the g-factor of the Ca^+ ion, with full account of the Breit interaction. The operators used for the g-factor evaluation can be found in reference [31], which include lowest order bound correction to the free electron g-factor QED contribution. All double excitations from the $n = 3$ and $n = 4$ shell up to the $6h$ shell have been included, representing 4109 jj configurations. Two independent calculations were performed, one that included the Coulomb interaction only in the Hamiltonian and one with inclusion of the Breit operator, which is then treated fully self-consistently on an equal footing with the Coulomb interaction. This lead to extra terms in both the Hamiltonian matrix from which are evaluated the configuration mixing coefficients and to the differential equations that are used to evaluate the wave functions. Convergence proved to be difficult in many cases, particularly when the Breit operator was treated self-consistently, while increasing the configuration space. In order to evaluate the uncertainty due to this difficult convergence, calculations with different number of convergence cycles were performed. The difference between the free and bound g-factor is plotted in Figure 11 for both calculations, as a function of the principal and angular quantum numbers n and ℓ of the highest shell to which the $n = 3$ and $n = 4$ electron have been excited. One easily sees that the effect of the Breit interaction increases with increasing correlation. It is also obvious from Figure 11 that convergence in n and ℓ is not quite reached for $6h$. The final value, including the Breit term is 2.0022564 (6)(12) where the first number in parenthesis represents the numerical uncertainty and the second one the convergence uncertainty. The difference with experimental value is 3×10^{-6}, well inside the theoretical error bars.

This agreement is however misleading, as we have not included two important effects. First single excitations have been left out, and second no excitations from $n = 1$ and 2 core orbitals have been included. The reason for leaving out the single excitation is due to the fact that the MCDF method is a variational procedure that minimizes an energy functional to obtain the wave function used to calculate the g-factor. In that case the Brillouin theorem (see, *e.g.*, [32]) states that single excitation does not contribute to the energy. In many cases, the addition of single excitation to the configuration space leads to a very unstable convergence, the MCDF code trying to converge to very different wave functions with identical energies. The inclusion of excitations from the core orbitals is possible and has been performed. However this leads to a very bad value of the g-factor, close of the single-configuration value. This is due to the fact that correlation orbitals must have large spatial overlap with the occupied orbitals that they correlate. Thus a $n = 5$ orbital that add correlation to the $4s$ when the $n = 1$ and 2 shell are closed will have an average radius close to the one of the $4s$, while the same orbital correlating the $1s$ if the core is open, will have a mean radius close to the one of the $1s$. Since the MCDF method uses an energy minimization procedure the correlation orbital will mostly contribute to the correlation of the inner shells, the gain in correlation energy being much larger in that case. This is observed in the calculation, noticing that the mean radii of all correlation orbital become of the same size as the radius of the $1s$ orbital when the $1s$ shell is open, while they are of the size of the $4s$ radius if all core orbital are closed. Since there are no more orbitals contributing to the correlation of the $4s$ the g-factor it is then not surprising that its value goes back to the Dirac-Fock value. The good agreement between theory and experiment just show that both effects (and the contribution of triple and higher excitations) cancel out to a large extent.

6 Outlook

The experimentally determined g_J-factor of Ca^+ fills a further gap of the measured Landé-factors of alkali-like ions. In Figure 12 we plotted these g_J-factors *vs.* the quantum number n. A third order polynomial function was fitted to the data. To our knowledge there exists no theoretical model which predicts the evolution of the g-factor of the alkali-like ions with increasing quantum numbers. However Figure 12 shows that collective electronic effects play an important role in these alkali-like systems. In principle the technique of the optical-microwave double method presented in our work on Ca^+ can also be applied to measure the g_J-factors of Sr^+ and Ra^+. The presence of a model describing how the g-factors change with increasing quantum number may help to predict the so far unknown values of the g_J-factors for these remaining alkali-like ions.

G.R. acknowledges support from the Fritz-Thyssen Stiftung. Our experiment was supported by the Deutsche Forschungsgemeinschaft.

References

1. G. Breit, Nature **122**, 649 (1928)
2. V.A. Dzuba *et al.*, Phys. Scripta **31**, 275 (1978)
3. E. Lindroth, A. Ynnerman, Phys. Rev. A **47**, 961 (1993)
4. T. Beier *et al.*, Phys. Rev. A **62**, 032510 (2000)
5. G. Werth, Phys. Scripta T **59**, 206 (1995)
6. R. Dicke, Phys. Rev. **89**, 472 (1953)
7. D.J. Wineland *et al.*, Phys. Rev. Lett. **50**, 628 (1983)
8. J.J. Bollinger *et al.*, Bull. Am. Phys. Soc. **37**(3), 1117 (1992)
9. G. Marx *et al.*, Eur. Phys. J. D **4**, 279 (1998)
10. W. Itano *et al.*, J. Opt. Soc. Am. B **2**, 1352 (1985)
11. F. Arbes *et al.*, Z. Phys. D **29**, 159 (1994)
12. P.A. Barton *et al.*, Phys. Rev. A **62**, 2503 (2000)
13. P. Indelicato *et al.*, Hyperf. Interact. **132**, 347 (2001)
14. S. Liaw, Phys. Rev. A **51**, R1723 (1995)
15. W.W. Smith, A. Gallagher, Phys. Rev. **145**, 26 (1966)
16. J. Jin, D.A. Church, Phys. Rev. Lett. **70**, 3213 (1993)
17. F. Arbes *et al.*, Z. Phys. D **7**, 295 (1993)
18. M. Knoop *et al.*, Phys. Rev. A **52**, 3763 (1995)
19. G. Savard *et al.*, Phys. Lett. A **158**, 247 (1991)
20. C. Lichtenberg *et al.*, Eur. Phys. J. D **2**, 29 (1998)
21. H.A. Schuessler, Appl. Phys. Lett. **18**, 11 (1971)
22. V. Enders *et al.*, J. Mod. Opt. **39**(2), 325 (1992)
23. F.G. Major, J.L. Duchène, J. Phys. France **36**, 953 (1975)
24. H.S. Lakkaraju, H.S. Schuessler, J. Appl. Phys. **53**, 3967 (1982)
25. N. Wiener, Acta Math. **55**, 117 (1930)
26. A. Khintchine, Math. Ann. **109**, 604 (1934)
27. H.A. Schuessler *et al.*, Phys. Rev. **187**, 5 (1969)
28. G. Tommaseo, Ph.D. thesis, University of Mainz, 2002
29. L.S. Brown, G. Gabrielse, Rev. Mod. Phys. **58**(1), 233 (1986)
30. E. Kienow *et al.*, Phys. Lett. A **46**, 441 (1974)
31. K. Cheng, W. Childs, Phys. Rev. A **31**, 2775 (1985)
32. C. Froese Fischer, *The Hartree-Fock Method for Atoms* (Wiley & Sons, New York, 1977)